

Kinetic Role of Reactive Intermediates in Controlling the Formation of Chlorine Dioxide in the Hypochlorous Acid–Chlorite Ion Reaction

Dávid Angyal, István Fábián, and Mária Szabó*

Cite This: *Inorg. Chem.* 2023, 62, 5426–5434

Read Online

ACCESS |



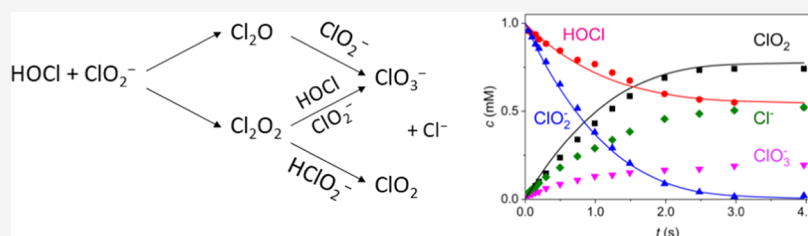
Metrics & More



Article Recommendations



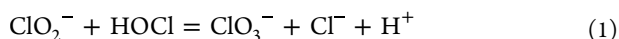
Supporting Information



ABSTRACT: An advanced experimental protocol is reported for studying the kinetics and mechanism of the complex redox reaction between chlorite ion and hypochlorous acid under acidic condition. The formation of ClO₂ is followed directly by the classical two-component stopped-flow method. In sequential stopped-flow experiments, the target reaction is chemically quenched using NaI solution and the concentration of each reactant and product is monitored as a function of time by utilizing the principles of kinetic discrimination. Thus, in contrast to earlier studies, not only the formation of one of the products but the decay of the reactants was also directly followed. This approach provides a firm basis for postulating a detailed mechanism for the interpretation of the experimental results under a variety of conditions. The intimate details of the reaction are explored by simultaneously fitting 78 kinetic traces, i.e., the concentration vs. time profiles of ClO₂⁻, HOCl, and ClO₂, to an 11-step kinetic model. The most important reaction steps were identified, and it was shown that two reactive intermediates have a pivotal role in the mechanism. While chlorate ion predominantly forms via the reaction of Cl₂O, chlorine dioxide is exclusively produced in reaction steps involving Cl₂O₂. This study leads to clear conclusions on how to control the stoichiometry of the reaction and achieve optimum conditions to produce chlorine dioxide and to reduce the formation of the toxic chlorate ion in practical applications.

1. INTRODUCTION

Practical applications and exotic kinetic phenomena have generated considerable interest in the chemistry of chlorite ion¹ that has been utilized as oxidizing agent in very diverse areas.^{2–10} Chlorite ion is also the precursor in the generation of chlorine dioxide,^{11–19} which has extensively been used in water and wastewater treatment technologies, cellulose bleaching, disinfection processes, deactivation of *Bacillus anthracis* spores, food industry, etc.^{13,20–34} In these systems, chlorine(I) always forms as an intermediate and, in turn, is involved in complex reactions with chlorite ion yielding Cl⁻, ClO₂, and ClO₃⁻ in variable concentration ratios depending on the actual conditions.^{35–40} According to earlier studies, the stoichiometry of this reaction is very sensitive to the pH, the concentrations as well as the concentration ratios of the reactants, and the presence of additional components that may act as promoters or inhibitors in the overall process. In general, the stoichiometry can be defined as the linear combination of eqs 1 and 2.

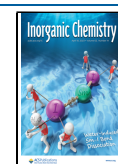


In addition to the practical aspects, understanding the kinetics and mechanism of the HOCl–ClO₂⁻ reaction is theoretically also challenging since it plays a central role in systematically designed chlorite-based chemical oscillators.^{38,41,42} Because of the inherent kinetic complexity of this system, well-defined reaction orders of the reactants and an explicit rate expression cannot be established for the overall process.

With respect to water treatment technologies and industrial processes, the primary concern is the formation of chlorate ion and other toxic byproducts when various chlorine species are used as disinfection and oxidizing agents.^{25,26,43–52} Toxicological studies confirmed that chlorate ion has antagonistic effects in living systems leading to renal insufficiency, methemoglobin formation, hemolysis, nephrotoxicity, and genotoxicity.^{53–56} The most challenging issue is how to limit the formation of this species at the possible lowest

Received: December 8, 2022

Published: March 28, 2023



concentration levels and achieve efficient production of chlorine dioxide at the same time. Adequate answers to this problem require understanding the intimate details of the corresponding processes.

The $\text{HOCl}-\text{ClO}_2^-$ reaction is relatively slow under alkaline condition and can easily be monitored by conventional kinetic techniques.^{35,39} However, it becomes increasingly faster by decreasing the pH and the use of fast kinetic methods is required in acidic solution.^{36,38,40,57,58} Kinetic studies on fast reactions mainly utilize some sort of an optical detection, and the single-wavelength stopped-flow (SF) method has become the workhorse in this field since the pioneering work of Hartridge and Roughton as well as Chance.^{59,60} Recent developments, i.e., the introduction of advanced diode array and CCD detectors combined with comprehensive data treatment algorithms, led to improved performance of the SF technique in terms of both spectral features and time resolution, thus broadening the scope of fast kinetic studies. Still, inherent limitations prevent the use of these instruments for studying composite reactions even if the corresponding reaction times are well within the SF time domain.

When the stoichiometry remains constant over the course of a reaction, measuring the concentration profile of only one component (reactant or product) may provide sufficient and reliable kinetic information even at one appropriately selected wavelength. However, complications arise when the stoichiometry is a function of time and monitoring the concentration change of each relevant species is not feasible. Such a situation may occur when (i) there are only weakly absorbing species, (ii) a strong absorbance band overlaps other spectral features, or/and (iii) the spectral changes are too complex, and the individual spectral contributions cannot be evaluated. Because of these constraints, the use of fast time-resolved spectroscopy is often of limited use for analyzing complex reaction mixtures.

In the $\text{HOCl}-\text{ClO}_2^-$ system, the most convenient way of monitoring the progress of the reaction has been the use of the SF method in two-component mixing mode at the characteristic spectral band of ClO_2 ($\lambda_{\text{max}} = 360 \text{ nm}$).^{38,41,58,61,62} However, the strong absorbance of this species overlaps with other spectral effects, and the obvious disadvantage of this approach is that the formation of only one of the final products is monitored. Thus, the SF results do not carry direct information on the concentration profiles of the reactants and other products. This leads to ambiguity in the interpretation of the experimental data because the stoichiometry is not constant over the entire course of the reaction. Consequently, the previously proposed kinetic models carry a substantial amount of uncertainty.

Earlier, we have shown that chemical quenching of a complex reactive system can successfully be used to circumvent the noted problems of spectrophotometric detection.^{63,64} In the iron(III)-catalyzed decomposition of chlorite ion, the reaction was stopped by adding fluoride ion in a pH 3.2 buffer to the reaction mixture at different reaction times. The quenching agent quickly and efficiently removed the catalyst and decreased the number of absorbing species from 7 to 2 by converting iron(III) into colorless fluoro complexes. Spectrophotometric and potentiometric analysis of the quenched reaction mixture made it possible to construct the concentration vs. time profiles for the reactants and products in the subsecond time domain. This rather arduous method provided specific kinetic information on the overall reaction, which was not accessible by the classical SF method.

In this study, we report an experimental protocol for monitoring the time-dependent concentration profiles of the individual species in the $\text{HOCl}-\text{ClO}_2^-$ reaction in the subsecond time domain using chemical quenching and kinetic discrimination. Based on the results, we provide a well-established kinetic model for the reaction, which clarifies specific details and resolves discrepancies in earlier reported results. The model can efficiently be used to predict the amount of chlorate ion formed in the system under various conditions. In a broader sense, these results also demonstrate that such a kinetic approach may provide a new insight into complex fast inorganic reactions and serve as a basis for detailed mechanistic studies.

2. EXPERIMENTAL SECTION

2.1. Materials. A chlorine-free sodium hypochlorite solution was prepared as described earlier.^{51,65} The purification of the stock solutions (eliminating chloride ions) was carried out by acidifying the sample with HClO_4 and adding AgClO_4 in appropriate amount. The AgCl precipitate was filtered off using a glass filter. Subsequently, NaOH was added to the solution to reach pH ~ 11.5 where the hypochlorite ion is stable. The remaining chloride ion contamination was measured by ion chromatography. It was always less than 1.5% of the total amount of OCl^- .

Commercial sodium chlorite (Fluka, $\sim 80\%$) was purified as reported earlier.^{38,66} The purity was determined by standard iodometric titration and found $>99\%$. Chlorine dioxide stock solution was prepared by mixing solid sodium chlorite with perchloric acid and transferring the evolving ClO_2 into a 1.0 mM HClO_4 ($I = 1.0 \text{ M NaClO}_4$) solution by a steady stream of argon gas.

All other chemicals were used without further purification. The reagent solutions were prepared with doubly deionized and ultrafiltered water obtained from an ELGA Purelab Classic water purification system. Sodium perchlorate was used to set the ionic strength to 1.0 M, and all experiments were carried out at $25.0 \pm 0.1^\circ\text{C}$.

2.2. Instrumentation. Iodometric titrations were made with a Metrohm 888 Titrando automatic titrator equipped with a Metrohm 6.0451.100 combination platinum electrode.

The pH was either calculated from the composition of the sample ($\text{pH} < 1.9$) or measured with a Metrohm 721 NET Titrino system equipped with a Metrohm 6.0262.100 combination glass electrode by converting the readout of the instrument into $\text{pH} = -\lg[\text{H}^+]$.⁶⁷ In the calculations, the acid dissociation of HClO_2 was taken into account using $\text{pK}_a = 1.82 \pm 0.04$ obtained in this work as described earlier.⁶⁶

To avoid the loss of chlorine dioxide from the stock solutions and the reaction mixtures, a home-built "shrinking bottle" was utilized in the experiments.^{68,69} The syringe of this device can be filled with a solution of ClO_2 or the reaction mixture by avoiding the headspace above the liquid phase. This arrangement assures that the concentration of the dissolved gas remains constant during dispensing of the solution. It was confirmed that the loss of chlorine dioxide was less than 0.5% over a day from the shrinking bottle.

Spectrophotometric experiments were made with an Agilent Technologies Cary 8454 UV–vis diode array spectrophotometer. It was confirmed that undesirable photochemical processes did not occur.⁷⁰

The concentrations of chloride, chlorate, and chlorite ion were determined using a Thermo Scientific Dionex ICS-5000⁺ ion chromatograph equipped with an AS – DV Dionex autosampler, a gradient pump (Dionex ICS-5000 DP), a conductivity detector (Dionex ICS – 3000/5000), and a 4 mm anion self-regeneration suppressor (Dionex AERS) operated in the auto-suppression recycle mode. A Dionex IonPac AS19 $4 \times 250 \text{ mm}$ analytical column was used in conjunction with a Dionex IonPac AG19 $4 \times 250 \text{ mm}$ guard column. A 25 μL injector loop and isocratic elution were applied using NaOH solution (0.020 M) at $1.0 \text{ mL} \times \text{min}^{-1}$ flow rate.

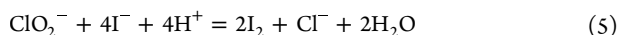
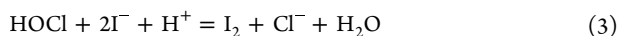
Kinetics measurements were performed with an Applied Photo-physics SX-20 sequential stopped-flow instrument using a 10.0 mm optical path length. Chlorine dioxide formation was monitored in the simple two-component mixing mode at 400 nm where other components do not contribute to the absorbance. The decay of HOCl and ClO_2^- was followed by utilizing the sequential mode of the instrument. In this case, the target reaction (i.e., the HOCl– ClO_2^- reaction) was triggered by mixing HOCl and ClO_2^- in a 1:1 ratio. After a certain incubation time, the reaction was quenched by mixing the reaction mixture with NaI solution also in a 1:1 ratio. The concentration profiles of the reactants and ClO_2 were obtained by combining these fast kinetic measurements as detailed in the subsequent chapter of this paper.

2.3. Molar Absorptivity of I_3^- and ClO_2 . The isosbestic wavelength of I_2 and I_3^- , 468 nm, was established by recording the spectra of acidic KIO_3 solutions containing large excess of KI in different concentrations. The molar absorptivity of iodine was determined in both the stopped-flow instrument and the spectrophotometer: $\epsilon_{\text{I}_2} = 711 \pm 1$ and $738 \pm 1 \text{ M}^{-1} \text{ cm}^{-1}$, respectively.

For the determination of the molar absorptivity of chlorine dioxide, the shrinking bottle was filled with a solution of ClO_2 . Then, a precisely known amount of this solution was injected into acidic sodium iodide solution and the iodine formed was titrated by standard iodometric method. Other portions of the ClO_2 solution were either transferred into the optical cell of the stopped-flow instrument or used to fully fill a standard quartz cuvette which was immediately sealed. The absorbance of these samples was measured at 400 nm. This procedure was repeated several times at different ClO_2 concentrations, and the molar absorbance was determined both in the SF instrument and the spectrophotometer: $\epsilon_{\text{ClO}_2} = 537 \pm 1$ and $548 \pm 1 \text{ M}^{-1} \text{ cm}^{-1}$, respectively.

The SF and spectrophotometric absorbance data were evaluated using the molar absorptivities determined in the given instrument.

2.4. Stoichiometric Experiments. The syringe of the shrinking bottle was filled with the reaction mixture immediately after mixing HOCl and chlorite ion reagent solutions. After about 5 min incubation time, an aliquot of the reaction mixture was transferred into a quartz cuvette and the concentration of chlorine dioxide was determined by spectrophotometry. Another portion was added to a neutral phosphate buffer ($\text{Na}_2\text{HPO}_4 = 4.8 \text{ mM}$, $\text{NaH}_2\text{PO}_4 = 1.2 \text{ mM}$) and purged with argon for 10 min to remove ClO_2 . Subsequently, HOCl was converted to Cl^- by adding I^- (eq 1). Since ClO_2^- and ClO_3^- do not oxidize I^- under such conditions, the concentration of HOCl was directly obtained from the amount of I_2 produced. The same sample was also used to determine the concentrations of Cl^- , ClO_2^- , and ClO_3^- by ion chromatography. The concentration of Cl^- produced in the target reaction was calculated as the difference of the measured Cl^- and the iodometrically determined HOCl concentrations. In control experiments, an aliquot of the reaction mixture was injected into acidic sodium iodide ion solution and the amount of iodine formed was obtained from spectrophotometric measurements at 468 nm. Within the experimental limitations, the same amount of I_2 was produced that was expected based on eqs 3 and 4 using the concentrations of HOCl, ClO_2 , and ClO_2^- from the other experiments. This confirms the dependability of the analytical protocol applied here.



It needs to be emphasized that the acid-catalyzed decomposition of ClO_2^- is orders of magnitude slower than the HOCl– ClO_2^- reaction and has negligible contribution to ClO_2 formation within the timescale of the experiments. Accordingly, all results are discussed by considering only the latter process.

3. RESULTS AND DISCUSSION

3.1. Stoichiometry. The stoichiometry of the HOCl– ClO_2^- reaction shows complex dependence on the conditions applied (cf. eqs 1 and 2), and it may also vary over the course of the reaction. In twofold excess of hypochlorous acid, the concentrations of the reactants and the products are independent of the pH at the end of the reaction (Figure S1). Under such conditions, chlorite ion completely disappears, and the concentration ratios of the products are practically the same.

Upon increasing the excess of chlorite ion over HOCl, the concentration of chlorine dioxide increases and eventually reaches a limiting value (Figure 1). Consequently, the relative amount of ClO_3^- , i.e., the concentration ratio of ClO_3^- and ClO_2 , decreases. At twofold excess of chlorite ion, HOCl is completely consumed.

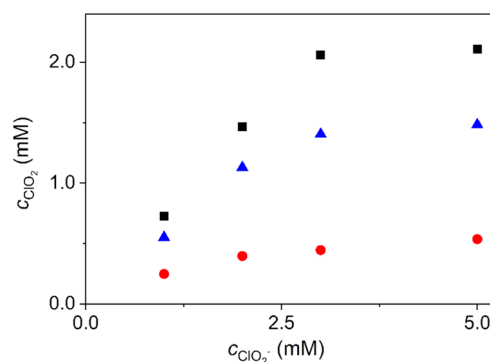


Figure 1. Concentration of the product ClO_2 in the HOCl– ClO_2^- reaction as a function of the chlorite ion concentration. ■, ClO_2 ; red ●, ClO_3^- ; blue ▲, Cl^- ; $c_{\text{HOCl}} = 1.0 \text{ mM}$, $\text{pH} = 2.0$, $T = 25.0 \text{ }^\circ\text{C}$.

Chloride ion has a profound effect on the reaction because it promotes the formation of chlorine dioxide over chlorate ion. The final concentrations of the products obtained from the kinetic experiments under the same conditions (*vide infra*) corroborate the results of the stoichiometric studies (Figure 2).

3.2. Kinetics. In conventional two-component stopped-flow experiments (SF), the solutions of HOCl and ClO_2^- of equal pH were mixed and the formation of chlorine dioxide was monitored at 400 nm. At the expense of some loss in

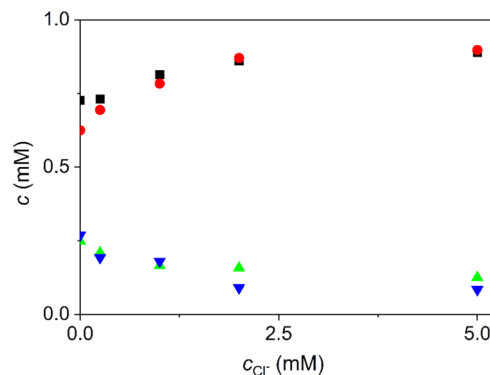


Figure 2. Effect of added chloride ion on the formation of ClO_2 and ClO_3^- . ClO_2 : ■ stoichiometric study, red ● kinetic study (at the end of the reaction), ClO_3^- : light green ▲ stoichiometric study, blue ▼ kinetic study (at the end of the reaction). $c_{\text{ClO}_2^-} = 1.0 \text{ mM}$, $c_{\text{HOCl}} = 1.0 \text{ mM}$, $\text{pH} = 2.0$, $T = 25.0 \text{ }^\circ\text{C}$.

sensitivity, this wavelength was selected instead of $\lambda_{\text{max}} = 360$ nm to avoid any spectral interference by the reactants. While ClO_3^- and Cl^- are nonabsorbing species, HOCl and ClO_2^- have overlying spectra and relatively weak contribution to the absorbance in the UV region, where ClO_2 is the dominant absorbing species. The noted contribution is not sufficient enough for the determination of the reactant concentrations even using multicomponent analysis of the spectra, i.e., time-resolved UV spectral experiments do not carry reliable information on the concentration profiles of the reactants and products.

As expected, composite kinetic features were observed at 400 nm, and the traces cannot be fitted to simple kinetic expressions. As shown in Figure 3, chloride ion catalyzes the

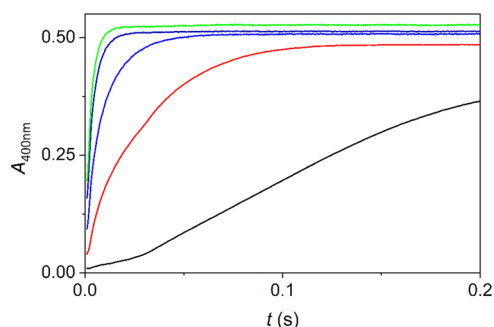
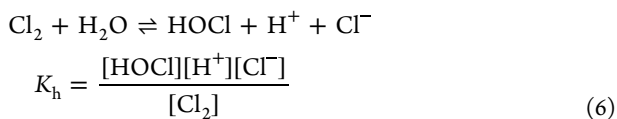


Figure 3. Kinetic traces of chlorine dioxide formation in the $\text{HOCl}-\text{ClO}_2^-$ reaction at different chloride ion concentrations (400 nm). Chloride ion was added to the HOCl reagent solution prior to mixing the reactants. Added Cl^- concentration: 0.0; 1.0; 2.0; 5.0; 30.0 mM (in the order of increasing absorbance at a reaction time) $c_{\text{ClO}_2^-} = 1.0$ mM, $c_{\text{HOCl}} = 3.0$ mM, $\text{pH} = 1.0$, $I = 1.0$ M (NaClO_4), $T = 25.0$ °C.

formation of chlorine dioxide. The actual shape of the kinetic curves depends on how the reactant solutions are assembled. When chloride ion is added to the solution of ClO_2^- , the kinetic traces start at the origin regardless of the concentration of chloride ion. However, when Cl^- is added to the HOCl solution, a clear absorbance jump is observed at the very beginning of the SF traces, which increases by increasing the concentration of Cl^- . This observation can be explained by considering that preliminarily chlorine is formed in the reagent solution in an equilibrium reaction (eq 6). It reacts much faster with ClO_2^- than HOCl and, consequently, fast ClO_2 formation occurs within the dead time of the SF experiments.



The correlation between the initially formed ClO_2 concentration and the initial chlorine concentration calculated by using the independently determined value of K_h at different Cl^- concentrations clearly supports this interpretation (Figure 4). To avoid the uncertainties associated with the very beginning of the SF traces, the initial ClO_2 concentration was calculated from the absorbance at 5 ms. The estimated hydrolytic constant based on these absorbance values, $-\lg K_h = 3.14 \pm 0.09$, is in excellent agreement with the result from our independent measurements (*vide infra*): $-\lg K_h = 3.18$.

The results also confirm that the hydrolytic equilibrium of Cl_2 is one of the key reaction steps in the overall process,

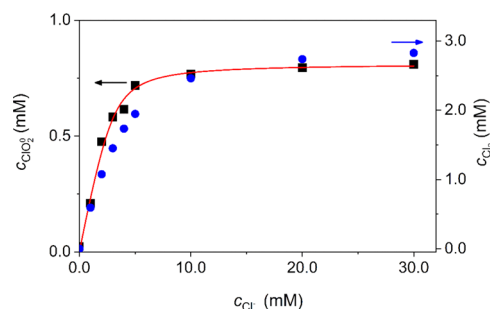


Figure 4. Effect of chloride ion concentration on the initial formation of ClO_2 in the $\text{HOCl}-\text{ClO}_2^-$ reaction. The initial ClO_2 concentration calculated from the absorbance at 5 ms when chloride ion is added to HOCl (■) and the result of fitting the data based on eq 6 (red —). The calculated initial concentration of Cl_2 using the value of K_h from the independent experiments is also shown (blue ●). $c_{\text{ClO}_2^-} = 1.0$ mM, $c_{\text{HOCl}} = 3.0$ mM, $\text{pH} = 1.0$, $I = 1.0$ M (NaClO_4), $T = 25.0$ °C.

which by no means should be considered as a fast preequilibrium reaction.

In the sequential stopped-flow experiments (SSF), the reactant solutions were mixed, and the target reaction was quenched in the second phase of the experiment with sodium iodide solution ($\text{pH} = 2.5$) after a predetermined incubation time. The formation of I_2 was monitored at 468 nm. The general description of the procedure is provided in the SI (Figure S2). A typical SF trace and the corresponding SSF trace are shown in Figure 5.

The kinetic trace in the SSF experiment exhibits an initial absorbance jump, ΔA_0 . This is due to the fast oxidation of iodide ion by HOCl and ClO_2 within the dead time of the

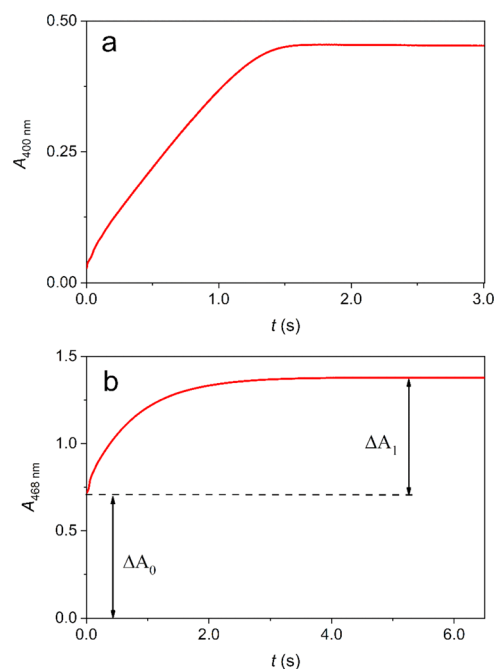


Figure 5. Kinetic traces recorded in the $\text{HOCl}-\text{ClO}_2^-$ reaction. The formation of ClO_2 in a simple two-component stopped-flow experiment (a) and the formation of I_3^- in the corresponding sequential stopped-flow experiment (b). Target reaction: $c_{\text{ClO}_2^-} = 1.0$ mM, $c_{\text{HOCl}} = 2.0$ mM, $\text{pH} = 2.0$, $I = 1.0$ M (NaClO_4), $T = 25.0$ °C. Quenching solution (SSF): $c_{\text{NaI}} = 0.3$ M, $\text{pH} = 2.5$.

stopped-flow instrument (eqs 3 and 4). The subsequent relatively slow process is the oxidation of I^- by ClO_2^- (eq 5). This is a simple first-order reaction under the conditions applied, the rate of which can easily be controlled by the pH. The measured absorbance change (ΔA_1) corresponds to the sum of the concentration of chlorite ion unreacted in the target reaction and generated by the reduction of ClO_2 (eq 2).

The kinetic traces from SF experiments can readily be converted into ClO_2 concentration by eq 7.

$$[\text{ClO}_2]_t = \frac{A_t^{400 \text{ nm}}}{\epsilon_{\text{ClO}_2}} \quad (7)$$

In the target reaction, the concentrations of HOCl and ClO_2^- were calculated from ΔA_0 and ΔA_1 by considering the twofold dilution of the reaction mixture during quenching.

$$[\text{HOCl}]_t = \frac{2\Delta A_0^{468 \text{ nm}}}{\epsilon_{\text{I}_2}} = -\frac{[\text{ClO}_2]_t}{2} \quad (8)$$

$$[\text{ClO}_2^-]_t = \frac{(\Delta A_{1468 \text{ nm}})}{\epsilon_{\text{I}_2}} - [\text{ClO}_2]_t \quad (9)$$

The concentrations of the other products, Cl^- and ClO_3^- , were calculated by utilizing the mass balance and redox balance equations (eqs 10 and 11)

$$\begin{aligned} & [\text{HOCl}]_0 + [\text{HClO}_2]_0 \\ &= [\text{ClO}_2]_t + [\text{ClO}_3^-]_t + [\text{Cl}^-]_t + [\text{HOCl}]_t + [\text{HClO}_2]_t \end{aligned} \quad (10)$$

$$\begin{aligned} & [\text{HOCl}]_0 + 3[\text{HClO}_2]_0 \\ &= 4[\text{ClO}_2]_t + 5[\text{ClO}_3^-]_t - [\text{Cl}^-]_t + [\text{HOCl}]_t + 3[\text{HClO}_2]_t \end{aligned} \quad (11)$$

In the target reaction, a small but typically negligible amount of Cl_2 is always present in accordance with eq 6. This species also rapidly oxidizes iodide ion (in 1:2 stoichiometric ratio) in the SSF experiments. It follows that $[\text{HOCl}]_t$ and $[\text{Cl}^-]_t$ correspond to the sum of the actual concentration of hypochlorous acid or chloride ion and the concentration of chlorine, respectively. This was considered during the fitting procedure.

The kinetics of the reaction was studied as the function of the concentrations of chlorite ion, hypochlorous acid, chloride ion, and the pH in detail (the experimental conditions are provided in Table S1). As demonstrated by Figure 6, the concentration vs. time profiles of the individual species could reliably be determined by the method described here. Further examples are shown in the SI (Figures S3–S7).

As expected, the stoichiometry of the reaction changes significantly within an individual kinetic run and as a function of the reactant concentrations (Figure 7). This clearly supports the basic premise of this study that monitoring the time profiles of each reactant and product is the prerequisite of developing a well-established kinetic model for this reaction.

The final concentrations of the reactants and their concentration ratios are in excellent agreement with the results obtained in the stoichiometric experiments (Figure 2). This also lends support to the reliability of the kinetic experiments. In general, the following trends were established. The formation of chlorine dioxide becomes faster and more

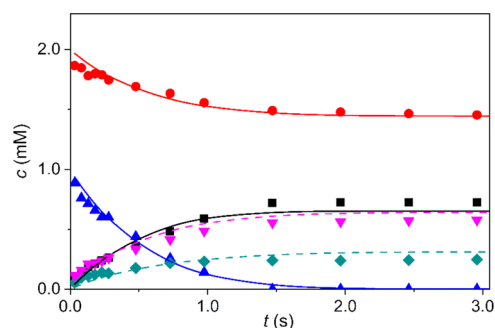


Figure 6. Concentrations of the reactants and products as a function of time in the $\text{HOCl}-\text{ClO}_2^-$ reaction. ■: ClO_2 ; red ●: HOCl ; blue ▲: ClO_2^- ; green ◆: ClO_3^- ; pink ▼: Cl^- . The solid lines are fitted kinetic traces obtained by simultaneous evaluation of 78 experimental concentration profiles of ClO_2 , HOCl , and ClO_2^- (cf. Table S1). The dashed lines are the simulated kinetic curves for ClO_3^- and Cl^- , which are also calculated by the fitting algorithm. $c_{\text{ClO}_2^-} = 1.0 \text{ mM}$, $c_{\text{HOCl}} = 2.0 \text{ mM}$, $\text{pH} = 2.0$, $I = 1.0 \text{ M}$ (NaClO_4), $T = 25.0 \text{ }^\circ\text{C}$.

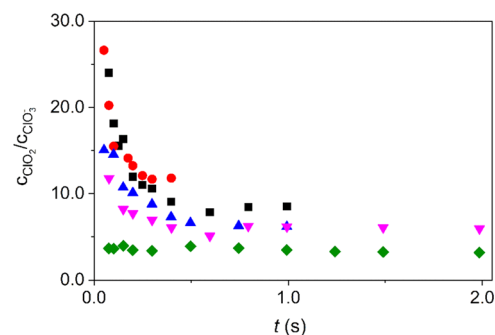


Figure 7. Effect of added Cl^- concentration on the concentration ratio of the products as a function of time. c_{Cl^-} : 0.0 mM (green ◆), 0.25 mM (pink ▼), 1.0 mM (blue ▲), 2.0 mM (■), 5.0 mM (red ●). $c_{\text{ClO}_2^-} = 1.0 \text{ mM}$, $c_{\text{HOCl}} = 1.0 \text{ mM}$, $\text{pH} = 1.0$, $I = 1.0 \text{ M}$ (NaClO_4), $T = 25.0 \text{ }^\circ\text{C}$.

significant by increasing the chloride ion concentration, decreasing the pH, and increasing the excess of chlorite ion over HOCl . This provides hints on how to optimize the ClO_2 formation and to minimize ClO_3^- formation in practical applications.

3.3. Mechanistic Considerations. The experimental results were evaluated by simultaneously fitting 78 kinetic traces (1065 concentration vs time data pairs) to a comprehensive kinetic model assembled based on earlier literature results. In these calculations, the kinetic model was represented by an ordinary differential equation system, which was integrated with the program package ZITA⁷¹ using the GEAR algorithm.⁷² It was assumed that each reaction step is elementary and follows either first- or second-order kinetics. The concentration vs. time profiles were calculated for each species, and the kinetic parameters were estimated by minimizing the differences between the measured and calculated concentrations of HOCl , ClO_2^- , and ClO_2 utilizing the built-in nonlinear least squares algorithm of the software.

First, the kinetic model included all previously proposed reaction steps with the originally reported rate constants (Table S2). A systematic analysis of the results revealed that quite a few reaction steps have no kinetic importance and can be eliminated from the model without affecting the goodness of the fit. It was concluded that 11 reaction steps are sufficient

Table 1. Kinetic Model for the ClO_2^- -HOCl Reaction

	reaction	rate constant		refs
		this study	literature	
R1	$2\text{HOCl} \rightleftharpoons \text{Cl}_2\text{O} + \text{H}_2\text{O}$	$k_1^{b,d}$	4.00×10^2	
		$k_{-1}^{a,d}$	3.48×10^4	
		K_1	1.15×10^{-2}	73
R2	$\text{Cl}_2 + \text{H}_2\text{O} \rightleftharpoons \text{HOCl} + \text{Cl}^- + \text{H}^+$	$k_2^{a,e}$	1.94×10^1	1.15×10^{-2} 8.70 $\times 10^{-3}$ 2.23×10^1 1.10×10^1 1.20×10^1
				74
				75
				76
				77
		$k_{-2}^{c,e}$	2.91×10^4	1.61×10^1 2.14×10^4 1.80×10^4
				75
				76
R3	$\text{HOCl} + \text{HClO}_2 \rightleftharpoons \text{Cl}_2\text{O}_2 + \text{H}_2\text{O}$	$-\lg K_2^f$	3.18	1.60×10^{5j} 4.34×10^4 3.36
		k_3^b	$(4.6 \pm 0.3) \times 10^2$	78
				74
				41
				40
R4	$\text{Cl}_2 + \text{HClO}_2 = \text{Cl}_2\text{O}_2 + \text{Cl}^- + \text{H}^+$	k_3^a	$(2.4 \pm 0.5) \times 10^1$	1.55×10^4 2.10×10^4 —
		k_4^b	$(4.4 \pm 1.0) \times 10^5$	64
		k_5^b	5.00×10^5	81
		k_6^b	$(2.9 \pm 0.2) \times 10^7$	1.00×10^5 1.30×10^5
		k_7^b	$(1.0 \pm 0.2) \times 10^5$	41
R5	$\text{Cl}_2 + \text{ClO}_2^- = \text{Cl}_2\text{O}_2 + \text{Cl}^-$			4.10×10^5 1.00×10^4 5.00×10^8 2.00×10^5
R6	$\text{Cl}_2\text{O} + \text{HClO}_2 = \text{Cl}_2 + \text{ClO}_3^- + \text{H}^+$			80
R7	$\text{Cl}_2\text{O}_2 + \text{ClO}_2^- = 2\text{ClO}_2 + \text{Cl}^-$			64
R8	$\text{Cl}_2\text{O}_2 + \text{HClO}_2 = 2\text{ClO}_2 + \text{Cl}^- + \text{H}^+$	k_8^b	$(3.4 \pm 0.3) \times 10^5$	1.50×10^9 1.20×10^4
R9	$\text{Cl}_2\text{O}_2 + \text{ClO}_2^- + \text{H}_2\text{O} = 2\text{HOCl} + \text{ClO}_3^-$	k_9^b	$(3.9 \pm 0.5) \times 10^4$	41
R10	$\text{Cl}_2\text{O}_2 + \text{HOCl} = \text{Cl}_2 + \text{ClO}_3^- + \text{H}^+$	k_{10}^b	1.00×10^4	41
R11	$\text{ClO}_2^- + \text{H}^+ \rightleftharpoons \text{HClO}_2$	$k_{11}^{b,g}$	1.00×10^{10}	
		$k_{-11}^{a,h}$	1.50×10^8	
		$\lg K_{11}^i$	1.82	1.74 1.72

^aFirst-order rate constant, s^{-1} . ^bSecond-order rate constant, $\text{M}^{-1} \text{s}^{-1}$. ^cThird-order rate constant, $\text{M}^{-2} \text{s}^{-1}$. ^dLower limit. ^eDetermined in separate experiments in this study and kept fixed during the fitting process. ^fCalculated from the forward and reverse rate constants obtained in this study. ^gEstimated value. ^hCalculated from k_{11} and K_{11} . ⁱDetermined in separate experiments in this study. ^jAt 50 °C.

for the interpretation of the experimental observations under the conditions applied (Table 1). It needs to be emphasized that the eliminated reaction steps could not be excluded based on preliminary considerations because most of them involve the same species that are reported in Table 1. Thus, a detailed sensitivity analysis was performed to reduce the kinetic model. To some extent, it is puzzling why so many unjustifiable reaction steps were postulated in the previous literature under similar conditions. Perhaps, analyzing the kinetic profiles of only one of the final products, ClO_2 , led to biased conclusions regarding the mechanism.

In our calculations, the acid–base equilibrium between ClO_2^- and HClO_2 (R11) was considered diffusion-controlled assuming $k_{11} = 10^{10} \text{ M}^{-1} \text{s}^{-1}$ and calculating the reverse rate constant as $k_{-11} = k_{11}/K_{11}$. The equilibrium constant for the formation of Cl_2O (R1) was taken from the literature and the corresponding rate constants were obtained as lower limits based on sensitivity analysis. When smaller values were used for these rate constants, the fitting process led to unrealistic results confirming that R1 is a preequilibrium step. The rate constants found here are considerably higher than those reported in the literature under slightly acidic conditions. This difference is consistent with earlier conclusions that R1 is acid-

catalyzed.⁷³ The forward and reverse rate constants for chlorine hydrolysis were determined in independent experiments in this study, $k_{\text{R2}} = 19.4 \pm 0.1 \text{ s}^{-1}$ and $k_{\text{R-2}} = (2.91 \pm 0.01)10^4 \text{ M}^{-2} \text{s}^{-1}$ (cf. SI) and introduced as fixed parameters in the fitting process. These results are in excellent agreement with previous results. In general, the standard deviation of the fitted rate constants in the kinetic model is less than 15%, which should be termed satisfactory by considering the complexity of the system. As demonstrated in Figures 6 and S2–S5, the reduced model provides excellent interpretation of the experimental kinetic traces.

Rate constants k_4 , k_5 , k_7 , and k_9 agree with earlier reported results within an order of magnitude; however, k_3 and k_8 differ by several orders of magnitude. Such discrepancies are not the consequence of different experimental conditions rather due to different interpretations of the results. In general, some of the rate constants may be altered significantly when a kinetic model is modified. There are profound differences between the kinetic models presented here and reported earlier. In contrast to earlier studies, our results confirm that R2 cannot be considered as a fast preequilibrium; R3 is a reversible reaction step; R6 is operative instead of the reaction of Cl_2O with ClO_2^- ; and the direct hydrolysis of Cl_2O_2 ($\text{Cl}_2\text{O}_2 + \text{H}_2\text{O} \rightarrow$

$\text{ClO}_3^- + \text{Cl}^- + 2\text{H}^+$) can be eliminated from the kinetic model. The latter step has been considered significant in earlier studies; therefore, we have thoroughly tested its feasibility. However, the inclusion of this step in the model either without steps R9 and R10 or with one of them led to considerably worse fitting results. The average deviation of the fitted and calculated data increased significantly and most of the rate constants became ill-defined. Again, we attribute the noted discrepancies to the limited information gained by monitoring only ClO_2 in the earlier studies.

According to the kinetic model, the competing reaction paths via the formation and subsequent reactions of the two reactive intermediates, Cl_2O_2 and Cl_2O , control the stoichiometry of the $\text{HOCl}-\text{ClO}_2^-$ reaction. Chlorine dioxide is exclusively produced in reactions involving Cl_2O_2 , R7, and R8. These steps are considerably faster than steps R9 and R10 that produces chlorate ion via the same intermediate. Thus, the reactions of Cl_2O_2 have a limited contribution to the formation of ClO_3^- and the main source of this product is step R6. It follows that increasing the transient concentration of Cl_2O_2 compared to Cl_2O promotes the formation of chlorine dioxide over chlorate ion. This finding is in line with the general trends noted earlier. By adding chloride ion to the system and decreasing the pH, the R2 equilibrium is shifted toward the formation of Cl_2 . Consequently, the concentration of HOCl becomes smaller and less Cl_2O is formed (R1), while step R4 becomes faster and more Cl_2O_2 is generated. Similarly, increasing the concentration of chlorite ion also makes the formation of the latter intermediate more favorable via steps R3 and R4.

4. CONCLUSIONS

The combined two-component and sequential stopped-flow experimental protocol made it possible to explore the intimate details of the $\text{HOCl}-\text{ClO}_2^-$ reaction. In contrast to earlier studies, not only the formation of one of the final products, ClO_2 , was monitored, but the time-dependent concentration profiles of all reactants and products were determined. These results provide a firm basis for postulating a detailed kinetic model for the interpretation of the experimental results under a variety of conditions. The most important reaction steps were identified, and it was shown that numerous irrelevant reaction steps were proposed in previous studies. This study leads to clear conclusions on how to control the stoichiometry of the reaction and achieve optimum conditions to produce chlorine dioxide in practical applications. Keeping the concentration of ClO_2^- in excess over HOCl and adding Cl^- to the reaction mixture enhances the formation of ClO_2 over chlorate ion. In general, the kinetic approach presented here could be beneficial in exploring the details of many complex redox reactions.

■ ASSOCIATED CONTENT

SI Supporting Information

The Supporting Information is available free of charge at <https://pubs.acs.org/doi/10.1021/acs.inorgchem.2c04329>.

Scheme of the sequential stopped-flow unit, concentrations of the reactants and products as a function of time and pH, reaction steps and the corresponding rate and equilibrium constants, and kinetics of chlorine hydrolysis (PDF)

■ AUTHOR INFORMATION

Corresponding Author

Mária Szabó – *ELKH-DE Mechanisms of Complex Homogeneous and Heterogeneous Chemical Reactions Research Group, University of Debrecen, Debrecen 4032, Hungary; Department of Inorganic and Analytical Chemistry, University of Debrecen, Debrecen 4032, Hungary; orcid.org/0000-0003-3575-1659; Email: szabo.maria@science.unideb.hu*

Authors

Dávid Angyal – *ELKH-DE Mechanisms of Complex Homogeneous and Heterogeneous Chemical Reactions Research Group, University of Debrecen, Debrecen 4032, Hungary; Doctoral School of Chemistry, University of Debrecen, Debrecen H-4032, Hungary*

István Fábián – *ELKH-DE Mechanisms of Complex Homogeneous and Heterogeneous Chemical Reactions Research Group, University of Debrecen, Debrecen 4032, Hungary; Department of Inorganic and Analytical Chemistry, University of Debrecen, Debrecen 4032, Hungary; orcid.org/0000-0002-4467-2912*

Complete contact information is available at:

<https://pubs.acs.org/doi/10.1021/acs.inorgchem.2c04329>

Notes

The authors declare no competing financial interest.

■ ACKNOWLEDGMENTS

This study was supported by the National Research, Development and Innovation Fund of Hungary under grant number OTKA-139140.

■ REFERENCES

- (1) The protolytic equilibrium between HClO_2 and ClO_2^- is established at a diffusion controlled rate. Consequently, the concentration ratio of the two forms is determined by the actual pH. In this paper, we use one name or formula – chlorite ion, ClO_2^- – for both the acidic and basic forms. Distinction between HClO_2 and ClO_2^- is made only when it is required for the clarity of the presentation.
- (2) Dereven'kov, I. A.; Shpagilev, N. I.; Valkai, L.; Salnikov, D. S.; Horvath, A. K.; Makarov, S. V. Reactions of aquacobalamin and cob(II)alamin with chlorite and chlorine dioxide. *J. Biol. Inorg. Chem.* **2017**, *22*, 453–459.
- (3) Hao, R. L.; Wang, X. H.; Liang, Y. H.; Lu, Y. J.; Cai, Y. M.; Mao, X. Z.; Yuan, B.; Zhao, Y. Reactivity of NaClO_2 and HA-Na in air pollutants removal: Active species identification and cooperative effect revelation. *Chem. Eng. J.* **2017**, *330*, 1279–1288.
- (4) Wang, X.; Jiang, S. J.; Cui, S.; Tang, Y. H.; Pei, Z. F.; Duan, H. R. Magnetic-controlled aerogels from carboxylated cellulose and MnFe_2O_4 as a novel adsorbent for removal of Cu(II) . *Cellulose* **2019**, *26*, 5051–5063.
- (5) Hao, R.; Wang, Z.; Mao, X.; Gong, Y.; Yuan, B.; Zhao, Y.; Tian, B.; Qi, M. Elemental mercury removal by a novel advanced oxidation process of ultraviolet/chlorite-ammonia: Mechanism and kinetics. *J. Hazard. Mater.* **2019**, *374*, 120–128.
- (6) Hao, R. L.; Song, Y. C.; Tian, Z. Y.; Li, Y. H.; Zhao, Y.; Wang, Z.; Gong, Y. P.; Ma, Z.; Qian, Z. Cooperative removal of SO_2 and NO using a cost-efficient triple-area control method. *Chem. Eng. J.* **2020**, *383*, 123164.
- (7) Hao, R.; Song, Y.; Tian, Z.; Li, Y.; Zhao, Y.; Wang, Z.; Gong, Y.; Ma, Z.; Qian, Z. Cooperative removal of SO_2 and NO using a cost-efficient triple-area control method. *Chem. Eng. J.* **2020**, *383*, 123164.

- (8) Zhou, X. Y.; Chen, X.; Liu, H. L. KI catalyzed C-H functionalization of acetone for the synthesis of 2-oxopropyl hetero-aromatic carboxylates. *Synth. Commun.* **2021**, *51*, 1–11.
- (9) Ma, J. X.; Zhao, Y.; Wei, Y. A. Performance and mechanism of oxidation, and removal of trace SeO₂ in flue gas utilizing a H₂O₂, NaClO₂, and Ca²⁺ slurry. *Environ. Sci. Pollut. Res.* **2021**, *28*, 42934–42944.
- (10) Kramar, A.; Ivanovska, A.; Kostic, M. Regenerated Cellulose Fiber Functionalization by Two-step Oxidation Using Sodium Periodate and Sodium Chlorite - Impact on the Structure and Sorption Properties. *Fibers Polym.* **2021**, *22*, 2177–2186.
- (11) Champ, T. B.; Jang, J. H.; Lee, J. L.; Wu, G.; Reynolds, M. A.; Abu-Omar, M. M. Lignin-Derived Non-Heme Iron and Manganese Complexes: Catalysts for the On-Demand Production of Chlorine Dioxide in Water under Mild Conditions. *Inorg. Chem.* **2021**, *60*, 2905–2913.
- (12) Wu, C. T.; Chang, C. Y.; Li, Y. Y.; Kuan, Y. L.; Lin, P. H. An efficiency analysis for the production of chlorine dioxide by the electrolysis of brine in seawater desalination plants. *Water Qual. Res. J.* **2019**, *54*, 127–133.
- (13) Zhou, S. Y.; Jin, T.; Sheen, S.; Zhao, G. H.; Liu, L. S.; Juneja, V.; Yam, K. Development of sodium chlorite and glucono delta-lactone incorporated PLA film for microbial inactivation on fresh tomato. *Food Res. Int.* **2020**, *132*, 109067.
- (14) Umile, T. P.; Groves, J. T. Catalytic Generation of Chlorine Dioxide from Chlorite Using a Water-Soluble Manganese Porphyrin. *Angew. Chem., Int. Ed.* **2011**, *50*, 695–698.
- (15) Isaza Ferro, E.; Perrin, J.; Dawson, O. G. J.; Vuorinen, T. Tertiary amine-catalyzed generation of chlorine dioxide from hypochlorous acid and chlorite ions. *Wood Sci. Technol.* **2021**, *55*, 67–81.
- (16) Yuan, B.; Mao, X. Z.; Wang, Z.; Hao, R. L.; Zhao, Y. Radical-induced oxidation removal of multi-air-pollutant: A critical review. *J. Hazard. Mater.* **2020**, *383*, 121162.
- (17) Hicks, S. D.; Xiong, S.; Bougher, C. J.; Medvedev, G. A.; Caruthers, J.; Abu-Omar, M. M. Mechanistic study of a manganese porphyrin catalyst for on-demand production of chlorine dioxide in water. *J. Porphyr. Phthalocyanines* **2015**, *19*, 492–499.
- (18) Su, R.; Huang, L.; Li, N.; Li, L.; Jin, B.; Zhou, W.; Gao, B.; Yue, Q.; Li, Q. Chlorine dioxide radicals triggered by chlorite under visible-light irradiation for enhanced degradation and detoxification of norfloxacin antibiotic: Radical mechanism and toxicity evaluation. *Chem. Eng. J.* **2021**, *414*, 128768.
- (19) Song, X.; Su, R.; Wang, Y.; Zhang, Y.; Gao, B.; Wang, Y.; Ma, D.; Li, Q. Visible light-driven chlorite activation process for enhanced sulfamethoxazole antibiotics degradation, antimicrobial resistance reduction and biotoxicity elimination. *Chem. Eng. J.* **2023**, *452*, 139103.
- (20) Nie, S.; Liu, X.; Wu, Z.; Zhan, L.; Yin, G.; Yao, S.; Song, H.; Wang, S. Kinetics study of oxidation of the lignin model compounds by chlorine dioxide. *Chem. Eng. J.* **2014**, *241*, 410–417.
- (21) Biswas, D.; Tiwari, M.; Tiwari, V. Comparative mechanism based study on disinfectants against multidrug-resistant *Acinetobacter baumannii*. *J. Cell. Biochem.* **2018**, *119*, 10314–10326.
- (22) Zhou, S. Y.; Hu, C. Y.; Zhao, G. H.; Jin, T.; Sheen, S.; Han, L.; Liu, L. S.; Yam, K. L. Novel generation systems of gaseous chlorine dioxide for *Salmonella* inactivation on fresh tomato. *Food Control* **2018**, *92*, 479–487.
- (23) Huang, C. X.; Zhang, B. D.; Wang, S. F.; Zhang, L. Y.; Wang, J.; Huang, X. Q.; Zhao, Y.; Huang, L. J. Moisture-triggered release of self-produced ClO₂ gas from microcapsule antibacterial film system. *J. Mater. Sci.* **2018**, *53*, 12704–12717.
- (24) Farinelli, G.; Giagnorio, M.; Ricceri, F.; Giannakis, S.; Tiraferri, A. Evaluation of the effectiveness, safety, and feasibility of 9 potential biocides to disinfect acidic landfill leachate from algae and bacteria. *Water Res.* **2021**, *191*, 116801.
- (25) Zhong, Y.; Gan, W. H.; Du, Y.; Huang, H.; Wu, Q. Y.; Xiang, Y. Y.; Shang, C.; Yang, X. Disinfection byproducts and their toxicity in wastewater effluents treated by the mixing oxidant of ClO₂/Cl⁻. *Water Res.* **2019**, *162*, 471–481.
- (26) He, G. L.; Zhang, T. Q.; Zheng, F. F.; Li, C.; Zhang, Q. Z.; Dong, F. L.; Huang, Y. Reaction of fleroxacin with chlorine and chlorine dioxide in drinking water distribution systems: Kinetics, transformation mechanisms and toxicity evaluations. *Chem. Eng. J.* **2019**, *374*, 1191–1203.
- (27) Sun, Y.; Niu, W.-K.; Hu, X.-J.; Ma, X.-H.; Sun, Y.-J.; Wen, Y. Oxidative degradation of polycyclic aromatic hydrocarbons in contaminated industrial soil using chlorine dioxide. *Chem. Eng. J.* **2020**, *394*, 124857.
- (28) Wang, Z.; Li, J.; Song, W.; Ma, R.; Yang, J.; Zhang, X.; Huang, F.; Dong, W. Rapid degradation of atrazine by a novel advanced oxidation process of bisulfite/chlorine dioxide: Efficiency, mechanism, pathway. *Chem. Eng. J.* **2022**, *445*, 136558.
- (29) Liu, B.; Niu, W.; Hu, X.; Liu, F.; Jiang, J.; Wang, H.; Wang, S. Enhanced oxidative activation of chlorine dioxide by divalent manganese ion for efficient removal of PAHs in industrial soil. *Chem. Eng. J.* **2022**, *434*, 134631.
- (30) Flagiello, D.; Erto, A.; Lancia, A.; Di Natale, F. Advanced Flue-Gas cleaning by wet oxidative scrubbing (WOS) using NaClO₂ aqueous solutions. *Chem. Eng. J.* **2022**, *447*, 137585.
- (31) Chen, M.; Chen, X.; Ray, S.; Yam, K. Stabilization and controlled release of gaseous/volatile active compounds to improve safety and quality of fresh produce. *Trends Food Sci. Technol.* **2019**, *95*, 33–44.
- (32) Singh, S.; Maji, P. K.; Lee, Y. S.; Gaikwad, K. K. Applications of gaseous chlorine dioxide for antimicrobial food packaging: a review. *Environ. Chem. Lett.* **2021**, *19*, 253–270.
- (33) Sun, X.; Baldwin, E.; Bai, J. Applications of gaseous chlorine dioxide on postharvest handling and storage of fruits and vegetables – A review. *Food Control* **2019**, *95*, 18–26.
- (34) Rastogi, V. K.; Ryan, S. P.; Wallace, L.; Smith, L. S.; Shah, S. S.; Martin, G. B. Systematic Evaluation of the Efficacy of Chlorine Dioxide in Decontamination of Building Interior Surfaces Contaminated with Anthrax Spores. *Appl. Environ. Microbiol.* **2010**, *76*, 3343–3351.
- (35) Taube, H.; Dodgen, H. Applications of Radioactive Chlorine to the Study of the Mechanisms of Reactions Involving Changes in the Oxidation State of Chlorine. *J. Am. Chem. Soc.* **1949**, *71*, 3330–3336.
- (36) Emmenegger, F.; Gordon, G. The rapid interaction between sodium chlorite and dissolved chlorine. *Inorg. Chem.* **1967**, *6*, 633–635.
- (37) Tang, T.; Gordon, G. Stoichiometry of the reaction between chlorite ion and hypochlorous acid at pH 5. *Environ. Sci. Technol.* **1984**, *18*, 212–216.
- (38) Peintler, G.; Nagypál, I.; Epstein, I. R. Systematic design of chemical oscillators. 60. Kinetics and mechanism of the reaction between chlorite ion and hypochlorous acid. *J. Phys. Chem. A* **1990**, *94*, 2954–2958.
- (39) Gordon, G.; Tachiyashiki, S. Kinetics and mechanism of formation of chlorate ion from the hypochlorous acid/chlorite ion reaction at pH 6–10. *Environ. Sci. Technol.* **1991**, *25*, 468–474.
- (40) Jia, Z.; Margerum, D. W.; Francisco, J. S. General-Acid-Catalyzed Reactions of Hypochlorous Acid and Acetyl Hypochlorite with Chlorite Ion. *Inorg. Chem.* **2000**, *39*, 2614–2620.
- (41) Kormányos, B.; Nagypál, I.; Peintler, G.; Horváth, A. K. Effect of Chloride Ion on the Kinetics and Mechanism of the Reaction between Chlorite Ion and Hypochlorous Acid. *Inorg. Chem.* **2008**, *47*, 7914–7920.
- (42) Shi, L.; Li, X. Simulation study of the chlorine dioxide–iodine–malonic acid oscillation reaction. *React. Kinet. Mech. Catal.* **2021**, *1261*–1280.
- (43) Wang, J. E.; Wu, Y. T.; Bu, L. J.; Zhu, S. M.; Zhang, W. Q.; Zhou, S. Q.; Gao, N. Y. Simultaneous removal of chlorite and contaminants of emerging concern under UV photolysis: Hydroxyl radicals vs. chlorate formation. *Water Res.* **2021**, *190*, 116708.

- (44) Han, J. R.; Zhang, X. R.; Li, W. X.; Jiang, J. Y. Low chlorine impurity might be beneficial in chlorine dioxide disinfection. *Water Res.* **2021**, *188*, 116520.
- (45) Chai, H. E.; Hwang, C. A.; Huang, L. H.; Wu, V. C. H.; Sheen, L. Y. Feasibility and efficacy of using gaseous chlorine dioxide generated by sodium chlorite-acid reaction for decontamination of foodborne pathogens on produce. *Food Control* **2020**, *108*, 106839.
- (46) Rubirola, A.; Boleda, M. R.; Galceran, M. T.; Moyano, E. Formation of new disinfection by-products of priority substances (Directive 2013/39/UE and Watch List) in drinking water treatment. *Environ. Sci. Pollut. Res.* **2019**, *26*, 28270–28283.
- (47) Tan, J. N.; Hwang, C. A.; Huang, L. H.; Wu, V. C. H.; Hsiao, H. I. In Situ Generation of Chlorine Dioxide for Decontamination of Salmonella, Listeria monocytogenes, and Pathogenic Escherichia coli on Cantaloupes, Mung Beans, and Alfalfa Seeds. *J. Food Prot.* **2020**, *83*, 287–294.
- (48) Lv, J.; Wang, Y.; Li, N. Oxidation of Citalopram with Sodium Hypochlorite and Chlorine Dioxide: Influencing Factors and NDMA Formation Kinetics. *Molecules* **2019**, *24*, 3065.
- (49) Rougé, V.; Allard, S.; Croue, J. P.; von Gunten, U. In Situ Formation of Free Chlorine During ClO₂ Treatment: Implications on the Formation of Disinfection Byproducts. *Environ. Sci. Technol.* **2018**, *52*, 13421–13429.
- (50) Sorlini, S.; Gialdini, F.; Biasibetti, M.; Collivignarelli, C. Influence of drinking water treatments on chlorine dioxide consumption and chlorite/chlorate formation. *Water Res.* **2014**, *54*, 44–52.
- (51) Csordás, V.; Bubnis, B.; Fábíán, I.; Gordon, G. Kinetics and Mechanism of Catalytic Decomposition and Oxidation of Chlorine Dioxide by the Hypochlorite Ion. *Inorg. Chem.* **2001**, *40*, 1833–1836.
- (52) Kong, Q.; Fan, M.; Yin, R.; Zhang, X.; Lei, Y.; Shang, C.; Yang, X. Micropollutant abatement and byproduct formation during the co-exposure of chlorine dioxide (ClO₂) and UVC radiation. *J. Hazard. Mater.* **2021**, *419*, 126424.
- (53) Ali, S. N.; Arif, H.; Khan, A. A.; Mahmood, R. Acute renal toxicity of sodium chlorite: Redox imbalance, enhanced DNA damage, metabolic alterations and inhibition of brush border membrane enzymes in rats. *Environ. Toxicol.* **2018**, *33*, 1182–1194 Article.
- (54) EFSA. Risks for public health related to the presence of chlorate in food. *EFSA J* **2015**, *13*, 4135.
- (55) Feretti, D.; Zerbini, I.; Ceretti, E.; Villarini, M.; Zani, C.; Moretti, M.; Fatigoni, C.; Orizio, G.; Donato, F.; Monarca, S. Evaluation of chlorite and chlorate genotoxicity using plant bioassays and in vitro DNA damage tests. *Water Res.* **2008**, *42*, 4075–4082 Article.
- (56) Steffen, C.; Wetzel, E. Chlorate poisoning: mechanism of toxicity. *Toxicology* **1993**, *84*, 217–231.
- (57) Yin, G. H.; Ni, Y. H. Quantitative description of the chloride effect on chlorine dioxide generation from the ClO₂–HOCl reaction. *Can. J. Chem. Eng.* **1998**, *76*, 921–926.
- (58) Nicoson, J. S.; Margerum, D. W. Kinetics and mechanisms of aqueous chlorine reactions with chlorite ion in the presence of chloride ion and acetic acid/acetate buffer. *Inorg. Chem.* **2002**, *41*, 342–347.
- (59) Hartridge, H.; Roughton, F. J. W.; Langley, J. N. A method of measuring the velocity of very rapid chemical reactions. *Proc. R. Soc. London, Ser. A* **1923**, *104*, 376–394.
- (60) Chance, B. Rapid and Sensitive Spectrophotometry. III. A Double Beam Apparatus. *Rev. Sci. Instrum.* **1951**, *22*, 634–638.
- (61) Kieffer, R. G.; Gordon, G. Disproportionation of chlorous acid. I. Stoichiometry. *Inorg. Chem.* **1968**, *7*, 235–239.
- (62) Nagypál, I.; Horváth, A. K. Compatible mechanism to characterize three independent but cross-coupled reactions of chlorite ion. *Chaos* **2015**, *25*, 064604.
- (63) Fábíán, I.; Gordon, G. Kinetics and mechanism of the complex formation of the chlorite ion and iron(III) in aqueous solution. *Inorg. Chem.* **1991**, *30*, 3994–3999.
- (64) Fábíán, I.; Gordon, G. Iron(III)-catalyzed decomposition of the chlorite ion: an inorganic application of the quenched stopped-flow method. *Inorg. Chem.* **1992**, *31*, 2144–2150.
- (65) Adam, L. C.; Fábíán, I.; Suzuki, K.; Gordon, G. Hypochlorous acid decomposition in the pH 5–8 region. *Inorg. Chem.* **1992**, *31*, 3534–3541.
- (66) Fábíán, I.; Gordon, G. Complex formation reactions of the chlorite ion. *Inorg. Chem.* **1991**, *30*, 3785–3787.
- (67) Irving, H. M.; Miles, M. G.; Pettit, D. L. A study of some problems in determining the stoichiometric proton dissociation constants of complexes by potentiometric titrations using a glass electrode. *Anal. Chim. Acta* **1967**, *38*, 475–488.
- (68) Silverman, R. A.; Gordon, G. Use of the syringe as a shrinking bottle. *Anal. Chem.* **1974**, *46*, 178.
- (69) Tóth, Z.; Fábíán, I. Kinetics and Mechanism of the Initial Phase of the Bromine–Chlorite Ion Reaction in Aqueous Solution. *Inorg. Chem.* **2000**, *39*, 4608–4614.
- (70) Fábíán, I.; Lente, G. Light-induced multistep redox reactions: The diode-array spectrophotometer as a photoreactor. *Pure Appl. Chem.* **2010**, *82*, 1957–1973 Article.
- (71) ZITA: A Comprehensive Program Package for Fitting Parameters of Chemical Reaction Mechanisms; Szeged: Hungary, 1999.
- (72) Hindmarsh, A. C. GEAR: Ordinary Differential Equation Solver. A.C. Hindmarsh; National Technical Information Service, 1974.
- (73) Beach, M. W.; Margerum, D. W. Kinetics of oxidation of tetracyanonickelate(II) by chlorine monoxide, chlorine, and hypochlorous acid and kinetics of chlorine monoxide formation. *Inorg. Chem.* **1990**, *29*, 1225–1232.
- (74) Sivey, J. D.; McCullough, C. E.; Roberts, A. L. Chlorine Monoxide (Cl₂O) and Molecular Chlorine (Cl₂) as Active Chlorinating Agents in Reaction of Dimethenamid with Aqueous Free Chlorine. *Environ. Sci. Technol.* **2010**, *44*, 3357–3362.
- (75) Furman, C. S.; Margerum, D. W. Mechanism of Chlorine Dioxide and Chlorate Ion Formation from the Reaction of Hypobromous Acid and Chlorite Ion. *Inorg. Chem.* **1998**, *37*, 4321–4327.
- (76) Eigen, M.; Kustin, K. The Kinetics of Halogen Hydrolysis. *J. Am. Chem. Soc.* **1962**, *84*, 1355–1361.
- (77) White, G. C. *Handbook of Chlorination and Alternative Disinfectants*; Van Nostrand Reinhold, 1992.
- (78) Sivey, J. D.; Bickley, M. A.; Victor, D. A. Catalysis of DBP-Precursor Bromination by Halides and Hypochlorous Acid, In *Recent Advances in Disinfection By-Products*, ACS Symposium Series, Vol. 1190, American Chemical Society, 2015; pp 251–269.
- (79) Horváth, A. K.; Nagypál, I.; Peintler, G.; Epstein, I. R.; Kustin, K. Kinetics and Mechanism of the Decomposition of Chlorous Acid. *J. Phys. Chem. A* **2003**, *107*, 6966–6973.
- (80) Rábai, G.; Beck, M. T. Kinetics and mechanism of the autocatalytic reaction between iodine and chlorite ion. *Inorg. Chem.* **1987**, *26*, 1195–1199.
- (81) Rábai, G.; Orbán, M. General model for the chlorite ion based chemical oscillators. *J. Phys. Chem. B* **1993**, *97*, 5935–5939.